JOURNAL OF CATALYSIS **177,** 363–377 (1998)
ARTICLE NO. CA982111

Ethylbenzene Hydroisomerization over Bifunctional Zeolite Based Catalysts: The Influence of Framework and Extraframework Composition and Zeolite Structure

L. D. Fernandes,*,† J. L. F. Monteiro,* E. F. Sousa-Aguiar,‡,§ A. Martinez,‖ and A. Corma‖,[1]

*NUCAT, Programa de Engenharia Química, PEQ/COPPE-UFRJ, Ilha do Fundão, CT, Bloco G, CP68502 Rio de Janeiro, Brazil; †DTQ/IT/UFRRJ, Antiga Estrada Rio São Paulo, km 47, CEP 23851-970, Seropédica, Rio de Janeiro, Brazil; ‡CENPES/PETROBRÁS, Divisão de Catalisadores, Ilha do Fundão, Quadra 7, CEP 21949-900, Rio de Janeiro, Brazil; §Escola de Química, UFRJ, Ilha do Fundão, CT. Bloco E, CEP 21499-900, Rio de Janeiro, Brazil; and ‖Instituto de Tecnología Química, ITQ/CSIC-UPV, Avenida de los Naranjos, s/n. 46022, Valencia, Spain

Received January 15, 1998; revised April 9, 1998; accepted April 17, 1998

The hydroisomerization of ethylbenzene (EB) has been carried out on a series of bifunctional Pt/Al_2O_3-zeolite catalysts, in which both the structure (mordenite, beta, Y, ZSM-5, MCM-22) and the chemical composition (for the mordenite and beta samples) of the zeolitic component were varied. Postsynthesis methods such as ion-exchange, steaming and chemical treatments were used to modify the composition of the samples (framework and extraframework Al content and nature of the compensation cation). Both parameters, zeolite structure and chemical composition, were seen to affect the activity and selectivity of the resultant catalysts. Large pore zeolites, particularly mordenite and beta, presented the highest selectivity to the desired isomerization products, i.e., xylenes. In the case of mordenites the textural properties (mainly the mesoporosity), played a key role in determining the activity and selectivity of the catalysts. Both, zeolite acidity and mesoporosity determined the amount of Brönsted sites accessible to the reactant molecules. It was seen that a reduced amount of accessible Brönsted acid sites in the zeolite favored the isomerization of EB with respect to secondary reactions like cracking of the naphthenes and dealkylation. Selectivities to xylenes above 40% at 60% EB conversion were obtained with most of the mordenite-based catalysts. Also, the calcium-exchanged mordenite samples gave larger xylene yields than the corresponding protonic samples. In the case of the Pt/Al_2O_3-beta samples, it was seen that formation of xylenes by isomerization of EB is favored in catalysts presenting a reduced density of Brönsted acid sites and a high mesoporosity. Thus, those catalysts prepared from the beta samples obtained by steaming and steaming + acid treatment of the original acidic zeolite were the most selective to xylenes, giving a selectivity close to 40% at ca 60% EB conversion.

Key Words: **hydroisomerization; ethylbenzene; xylenes; zeolite; beta; mordenite; faujasite; dealumination.**

1. INTRODUCTION

The isomerization of the C_8 aromatic fraction is an acid-catalyzed process of great interest for the petrochemical industry, mainly due to the increasing demand for *p*-xylene to be used for the production of polyesters resins (1). This fraction is usually obtained from naphtha reforming and contains ethylbenzene (10–60%) plus xylene isomers in a composition close to the thermodynamic equilibrium (para/meta/ortho = 1/2/1). Since the boiling points of the C_8 isomers are too close to make their separation by distillation feasible, *p*-xylene is usually separated from the other components by fractional crystallization or by selective adsorption using molecular sieves. The raffinate, now poor in *p*-xylene, is isomerized and in order to avoid ethylbenzene holding up in the process, it is most desirable either to isomerize the ethylbenzene to xylenes or, as a second option, to carry out its dealkylation/transalkylation into products which can be easily separated.

While xylene isomerization can proceed over acid catalysts, ethylbenzene isomerization can only take place in the presence of bifunctional catalysts, presumably through a mechanism involving partially hydrogenated intermediates like alkylcyclohexenes (2–5). Nowadays, there is an increasing trend to use bifunctional catalysts in the presence of hydrogen co-feed to isomerize the C_8 aromatic fraction. Besides the possibility of carrying out ethylbenzene conversion, these catalysts are more stable to deactivation by coking than the monofunctional ones.

Many bifunctional catalysts commercially used to isomerize the C_8 aromatic fraction contain a zeolitic component (either mordenite or ZSM-5), in combination with a noble metal (platinum) supported on alumina or silica-alumina, where the metal provides the hydrogenation/dehydrogenation function. Although mordenite has the potential advantage of hydroisomerizing ethylbenzene into

[1] To whom correspondence should be addressed. E-mail: acorma@itq.upv.es.

0021-9517/98 $25.00

xylenes, the results obtained up to now show that there is some room for improvement (6–13). On the other hand, ethylbenzene is converted over ZSM-5-based catalysts mainly by dealkylation, thus producing large amounts of benzene and light hydrocarbons (14), although there has been a recent claim (15) that the use of ZSM-5 with high Si/Al ratios may suppress the dealkylation reaction.

Most of the reports on ethylbenzene isomerization over zeolite-containing catalysts refer to ZSM-5 (1, 12–13, 15, 17), Y (1, 16–18), or mordenite (1, 6–11, 18) as the zeolitic component of the catalyst. On the other hand, although zeolite beta has wide channels to accommodate the hydrogenated intermediates without diffusion constraints and presents no large cages which could enhance disproportionation reactions, we are not aware of any publication in the open literature using this zeolite for the isomerization of ethylbenzene.

The aim of this work was to study the hydroisomerization of ethylbenzene over a series of bifunctional catalysts based on two large pore zeolites having different crystalline structures, mordenite and beta, which were prepared in a wide range of framework and extraframework compositions. Besides those zeolites, individual samples of ZSM-5, MCM-22, and zeolite Y have also been used in order to investigate the effect of pore structure on the hydroisomerization, dealkylation, and transalkylation reactions. Additionally, and in order to study the influence of the acid strength on the isomerization selectivity, some calcium-exchanged mordenite samples were evaluated.

2. EXPERIMENTAL

2.1. Preparation of Catalysts

The parent mordenite sample was a commercial sodium mordenite (NaM) from PQ Corporation (VALFOR CP500-11) having a SiO_2/Al_2O_3 ratio (SAR) of 10.7, as measured by X-ray fluorescence (XRF), and no EFAL species, as indicated by ^{27}Al MAS NMR.

The NaM sample was converted into the acid form by ion-exchange with a 0.5 *M* hydrochloric acid solution ($H^+/Na^+ = 2.0$) at 298 K for 1 h (sample HM000). The exchanged sample was hydrothermally treated at 823 K in a tubular furnace under 100% steam for 2 h (sample HM201). Part of this sample was acid-leached with a 4 *M* hydrochloric acid solution under reflux for 2 h using an acid to zeolite ratio of 30 cm^3/g to produce sample HM211. The latter was submitted to two additional cycles of steaming + acid leaching to obtain a highly dealuminated mordenite (sample HM213). These cycles were similar to the previous one, except for the steaming temperature (873 and 923 K for the 2nd and 3rd cycles, respectively). Sample HM000 was also acid-washed with a 1.0 *M* HCl solution under reflux for 3 h (sample HM010). Some of the protonic mordenite samples were cation-exchanged with a calcium acetate aqueous solution (0.2 *M*, 6 h under reflux). After the exchange the samples were washed with deionized water and dried at 373 K overnight. The degree of exchange was ca 75% for CaHM000, 80% for CaHM211, and 60% for CaHM213, as determined by chemical analyses.

The parent zeolite beta was a commercial TEA-β from PQ Corporation (VALFOR CP806B25), with a SAR of 23, as determined by XRF.

The acid form of zeolite β (sample Hβ000) was generated by air calcination of TEA-β at 773 K for 3 h in order to remove the template. This process was followed by ion-exchange with a 2.0 *M* ammonium chloride solution ($NH_4^+/Al = 7.0$) at 353 K for 2 h and a final calcination at 773 K for 3 h. Portions of this sample were then dealuminated by using three different procedures: (1) hydrothermal treatment with 100% steam at 873 K for 3 h (sample Hβ301), (2) acid treatment with a 0.1 *M* hydrochloric acid solution under reflux for 2 h and an acid/zeolite ratio of 30 cm^3/g (sample HClβ), and (3) slow addition (12 cm^3/h) of a 0.3 *M* ammonium hexafluorosilicate (HFS) solution to a suspension of the zeolite in a 5.0 *M* ammonium acetate buffer solution, subsequently held at 368 K for 8 h (sample HFSβ). Samples Hβ311 and Hβ-HFS were prepared, respectively, by leaching Hβ301 with HCl and by treating Hβ000 with HFS as previously described, aiming at the removal of the extraframework alumina (EFAL) from the latter sample.

The zeolite Y sample (USY311) was prepared from a NaY sample having a SAR = 5.6 and synthesized according to the procedure described in Ref. (19). The NaY sample was first ion-exchanged with a 3.5 *M* ammonium chloride solution ($NH_4^+/Al = 10.0$), followed by hydrothermal treatment at 923 K for 1 h and leaching with a 1.0 *M* sulfuric acid solution at 343 K in such a way as to keep the pH of the slurry always above 3.

The ZSM-5 sample was obtained by converting a commercial sample from PQ Corporation (CBV3020, NH_4^+ form) to its acidic form by calcination at 823 K for 3 h under air.

The MCM-22 sample was prepared following the procedure reported in Ref. (20) and using hexamethyleneimine as template. The as-synthesized sample was converted into the acid form by calcination under air at a heating rate of 2 K/min, being successively held at 423 K for 150 min, 623 K for 180 min, and finally at 853 K for 5 h.

The bifunctional catalysts were obtained by intimately mixing the zeolites with a Pt/Al_2O_3 sample in the adequate proportions to give the desired overall platinum content. The Pt/Al_2O_3 (0.6 wt% Pt) was prepared by impregnation of a γ-Al_2O_3 (Merck) with the required amount of hexachloroplatinic acid dissolved in a 0.2 *M* hydrochloric acid solution. The slurry was dried in a rotavapor and calcined at 773 K for 3 h. The Pt/Al_2O_3 sample presented a BET area of 118 m^2/g and a metallic area of 1.2 m^2/g as

determined by N_2 adsorption and H_2 chemisorption, respectively. A mordenite-based catalyst containing 1.0 wt% Pt was prepared in a similar way by mixing the zeolite with a Pt/Al_2O_3 (2.0 wt% Pt).

2.2. Catalyst Characterization

The chemical composition of the samples was measured by X-ray fluorescence (XRF) using a Phillips PW1407 spectrometer. X-ray diffraction analyses were performed with a Phillips PW1729 diffractometer, using monochromized CuK_α radiation at 40 kV and 40 mA, and a scanning rate of 0.1° (2θ)/s. Crystallinity was calculated by comparing the areas under selected peaks of the diffractograms (those between $2\theta = 5$–31.6° for the mordenite samples and that at ca 22° for the zeolite β samples) to the corresponding ones of NaM and TEA-β, and considering the latter samples as 100% crystalline.

Textural properties were determined from N_2 physisorption at 77 K in a Micromeritics ASAP 2400 apparatus. Before measurements, the samples were pretreated in vacuum at 573 K for 3 h.

Solid-state ^{29}Si and ^{27}Al NMR spectra were collected in a Varian VXR-300 FT NMR spectrometer at 7.05 T, equipped with a Varian CP-MAS probe. The ^{29}Si MAS NMR spectra were obtained at 59.8 MHz using 8.2 μs ($\pi/2$) pulses and 20-s delay, a total of 500 pulses being accumulated. The magic angle spinning speed was 3 kHz. The ^{27}Al MAS NMR spectra were obtained at 78.4 MHz using 0.7 μs ($\pi/15$) pulses and 0.2-s delay, a total of 3000 pulses being accumulated. The magic angle spinning speed was 7 kHz. The ^{27}Al NMR spectra were recorded before and after washing the samples with a 38% ethanolic solution of acetylacetone (ACAC). This treatment was carried out to try to account for all the Al species, including the so-called NMR "invisible" ones.

The surface zeolite composition was measured by X-ray photoelectron spectroscopy (XPS). The XPS spectra were recorded at room temperature using a Perkin Elmer model 1257 spectrometer with a hemispherical analyzer operated with a MgK_α X-ray source ($h\nu = 1253.6$ eV).

A Nicolet 710 FTIR spectrometer was used to measure the acidity of the samples. Self-supported wafers with 10 mg/cm^2 were pretreated overnight under vacuum at 673 K and cooled down to room temperature. After acquisition of the spectrum in the OH stretching region, pyridine vapor (6.6 kPa) was admitted to the cell until equilibium was reached. Next, the samples were heated consecutively under vacuum to 523, 673, and 723 K with spectra acquisition at room temperature after each desorption treatment.

TEM analyses obtained with a Jeol JEM-2000 FX transmission electron microscope showed that the size of the crystallites of the parent NaM sample was about 0.40 μm and that the parent TEA-β sample was formed by aggregates of very small crystallites with ca 200 Å diameter.

Acid properties of the mordenite and beta samples were also monitored by using *n*-heptane cracking as a model reaction. The experiments were done in a glass tubular reactor at 623 K, a WHSV in the 0.5–5.0 h^{-1} range, and a hydrogen/*n*-heptane molar ratio of 65. The products were analyzed "on line" by gas chromatography with a CP-SIL-5CB column and a FID.

2.3. Catalytic Evaluation

The bifunctional catalysts, formed by the Pt/Al_2O_3-zeolite mixture, were pelletized, crushed, and sieved to 0.59–0.84 mm particles. Before starting the reaction, the catalysts were submitted to an "*in situ*" calcination at 773 K under nitrogen flow, followed by reduction at 723 K under hydrogen flow. The ethylbenzene isomerization reaction was performed in a stainless steel tubular reactor at 15 bar total pressure, hydrogen/ethylbenzene ratio of 5.0 (mol/mol), and temperatures in the 653–693 K range. The space velocity (WHSV, based on the weight of zeolite) was varied between 5–100 h^{-1} in order to obtain different ethylbenzene conversions. Products were analyzed "on line" in a GC equipped with a 60-m length CP-WAX capillary column and a FID.

3. RESULTS AND DISCUSSION

3.1. Characterization of the Catalysts

In Table 1 the treatments used to obtain the different zeolite samples and their nomenclature, chemical composition, and crystallinity are given. It can be seen there that the bulk SAR for sample HM000 is higher than that of the parent NaM sample, showing that some dealumination occurred during the ion-exchange step with HCl. In fact, when ^{27}Al MAS NMR was carried out a sharp signal at ca 0 ppm was observed besides the band at ca 55 ppm assigned to tetrahedral Al, indicating that some highly dispersed EFAL species remained trapped in the pores of the HM000 zeolite. The different framework SAR values obtained from ^{29}Si NMR and ^{27}Al NMR indicate that this sample contained silanol groups in the vacant sites left behind after aluminium extraction. This was confirmed by ^{29}Si NMR/CP. Indeed, Si–OH groups present a signal in the ^{29}Si NMR spectra that overlaps with the Si(1Al) signal, resulting in artificially low lattice SAR values calculated from ^{29}Si NMR data. Moreover, the SAR determined from XPS is higher than both the bulk and the framework SAR due to the preferential dealumination of the zeolite surface. Dealumination of HM000 by hydrothermal treatment (sample HM201) increased the framework SAR from ca 13 to 53, while the surface SAR value determined by XPS decreased to ca 12, indicating that some migration of EFAL species to the outer shell of the zeolite crystallites has occurred during the steam treatment. This effect was accompanied by the appearance of broad bands at ca 0 and 30 ppm in the ^{27}Al MAS NMR

TABLE 1

Chemical Composition, XRD Crystallinity, and Treatments Performed to Obtain the Different Samples

Sample	Treatments	SAR				Crystallinity (%)
		Bulk	^{29}Si NMR	^{27}Al NMR	XPS	
HM000	Ion exchange of Na-mordenite with 0.5 *M* HCl	12.5	13.2	15.7	26.7	99
HM010	Acid leaching of HM000 with 1.0 *M* HCl	16.7	—	—	—	86
HM201	Hydrothermal treatment of HM000 at 823 K	12.3	53.2	20.2	11.7	112
HM211	Acid leaching of HM201 with 4.0 *M* HCl	69.3	79.4	73.7	82	121
HM213	3 × (hydrothermal + acid) treatment of HM000	125.1	236	258	102	123
Hβ000	Calcination of TEA-β at 773 K, ion exchange with NH_4Cl and a final calcination at 773 K	25.6	48.8	39.6	32.6	83
Hβ301	Hydrothermal treatment of Hβ000 at 873 K	25.6	72.8	52.7	31.9	75
Hβ311	Acid leaching of Hβ301 with 0.1 *M* HCl	71.2	30.8	106	93.5	70
HCLβ	Acid leaching of Hβ000 with 0.1 *M* HCl	64.7	—	—	68.0	83
Hβ-HFS	HFS treatment of Hβ000 (for EFAL removal only)	32.3	19.2	32.3	36.0	77
HFSβ	HFS treatment of Hβ000 (for lattice aluminum removal)	56.6	—	—	28.4	60
USY311	Ion exchange of NaY with NH_4Cl, hydrothermal treatment at 923 K and acid leaching with H_2SO_4	7.6	11.2	11.1	8.0	—
ZSM-5	Calcination at 823 K of an NH_4ZSM-5 sample	53.8	—	—	—	—
MCM-22	Calcination at 853 K for 5 h of the as-made sample	30.0	—	—	—	—

spectrum of HM201, which are usually assigned to different kinds of EFAL species presenting octahedral and pentahedrally or tetrahedrally distorted coordination, respectively (21, 22). Treatment of this sample with a HCl 4.0 *M* solution (sample HM211) results in removal of EFAL species, together with some extraction of framework Al, as observed from the increase of the bulk and framework SAR values, while a strong reduction of the EFAL bands in the ^{27}Al MAS NMR spectrum was evidenced (not shown). Finally, a severe dealumination of the mordenite accompanied by some surface Al enrichment was observed after submitting the parent HM000 sample to three consecutive cycles of steam + acid treatments (sample HM213).

In the case of the zeolite beta series, the SAR of sample Hβ000 calculated from ^{29}Si MAS NMR (SAR = 48.8) is significantly higher than that of the bulk (SAR = 25.6), indicating that a significant amount of EFAL species were generated during the initial calcination step performed to eliminate the template. Indeed, a sharp signal at ca 0 ppm was observed in the ^{27}Al NMR spectra of Hβ000 (Fig. 1a), which might be ascribed to the presence of a highly dispersed octahedral EFAL phase. A broadening of this band after impregnation with ACAC was an indication that the so-called "invisible" aluminium species were present. All these species were effectively removed after the HFS treatment, since only the signal at ca 55 ppm could be observed in the ^{27}Al NMR spectrum of sample Hβ-HFS. On the other hand, steam dealumination of Hβ000 further increased the amount of EFAL species, as may be inferred from the much greater difference between the bulk and the framework SAR observed for sample Hβ301. Besides that, a broad band at ca 30 ppm assigned to pentacoordinated or tetrahedrally distorted EFAL species appeared in the

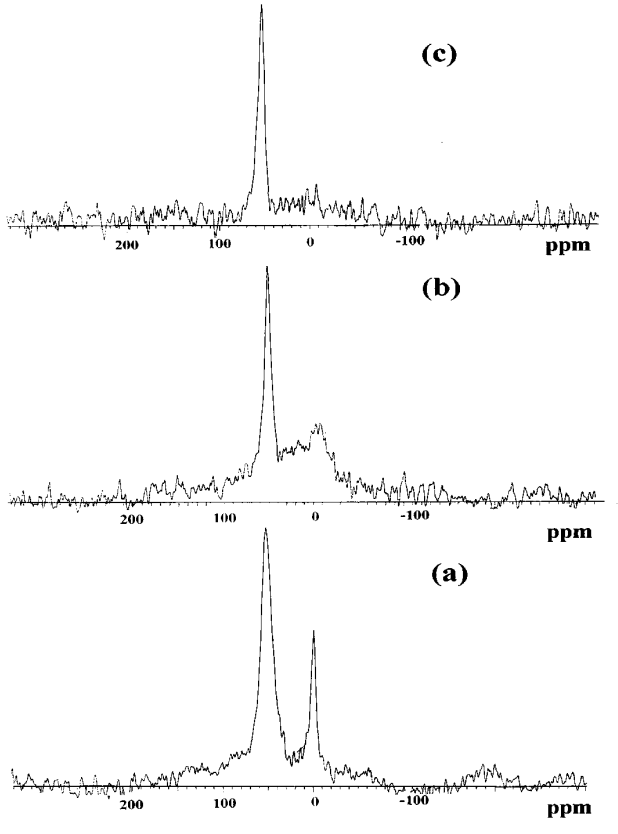

FIG. 1. ^{27}Al NMR spectra of the beta samples. (a) Hβ000, (b) Hβ301, and (c) Hβ311.

^{27}Al NMR spectrum of sample Hβ301 (Fig. 1b). Acid leaching of Hβ301 removed most, but not all, of the EFAL species, since although only the peak at ca 55 ppm corresponding to framework Al^{IV} could be observed in the ^{27}Al NMR spectrum of Hβ311 (Fig. 1c), a small peak appeared at ca 0 ppm after ACAC impregnation. It has to be noted in Table 1 that the acid-treated Hβ311 and HCLβ samples presented unusually low SAR values calculated from ^{29}Si NMR, something which can be ascribed to the high concentration of silanol groups generated during the acid treatments. This is due to the fact that the ^{29}Si NMR signal of Si(3Si, 1OH) groups (Q^3) appearing at ca -104 ppm overlaps with the signal of Si(3Si, 1Al), thus making the value of the framework SAR calculated by NMR artificially low.

Sample USY311 had a rather uniform global composition, and the NMR data indicate that some of the Al extracted from the framework in the hydrothermal treatment was not acid-leached.

The textural characteristics of the samples, as well as their acidity measured by IR spectroscopy with adsorption–desorption of pyridine, are given in Table 2.

The results show that most of the pore volume in HM000 can be attributed to micropores, with only a marginal contribution of the mesopores. However, a progressive formation of mesopores upon dealumination can be observed for the mordenite series. Dealumination by steam treatment decreased the surface area of the HM000 sample, which may have been caused by pore plugging due to condensed EFAL species, as suggested by the increase in surface area and pore volume experienced after acid leaching of HM201 (sample HM211). Further dealumination by three consecutive cycles of steam + acid treatments (sample HM213) decreased the surface area of the zeolite but increased the contribution of the mesopores to the total pore volume. Moreover, acid leaching of HM000 (sample HM010) did not change appreciably either the surface area or the pore volume of the zeolite.

On the other hand, all the zeolite β samples showed a much higher mesoporosity as compared to the mordenites (Table 2). Even the original TEA-β sample presents high values of mesopore area and pore volume. The small size of the crystallites of this sample and the shape of the hysteresis loop in the adsorption isotherms suggests that most of its mesoporosity is associated with intercrystalline voids. The mesopore volume was substantially reduced when the original zeolite was dealuminated by either acid (sample HClβ) or HFS (sample HFSβ) treatments. As shown in Table 2, even the mild treatment of Hβ000 sample with ammonium hexafluorosilicate (sample Hβ-HFS), which was carried out to selectively remove EFAL species, decreased the micro- and mesopore volume. This could be an indication of some silica deposition during the HFS treatments as already reported by Wang *et al.* (23).

From the IR spectra (Fig. 2), it could be observed that after adsorbing pyridine and desorbing at 523 K, only a fraction of the hydroxyls vibrating at ca 3610 cm^{-1} interacts with the base in the case of the HM000, HM010, and HM201 samples, suggesting that part of the Brønsted acid

TABLE 2

Textural Properties and Acidity of the Zeolites as Measured by IR with Adsorption of Pyridine and Desorption at Different Temperatures

Sample	BET area (m^2/g)	Pore volume (cm^3/g)		Acidity (μmol/g)[a]					
				Brønsted			Lewis		
		Meso	Micro	523 K	623 K	673 K	523 K	623 K	673 K
HM000	447	0.03	0.20	30.9	26.2	16.6	9.6	21.7	12.0
HM010	424	0.04	0.19	31.6	17.8	7.1	15.7	20.4	18.7
HM201	398	0.07	0.17	8.1	2.8	—	6.0	4.1	3.8
HM211	485	0.12	0.19	12.8	9.0	—	3.8	3.1	—
HM213	433	0.14	0.15	2.8	1.9	—	4.1	3.1	—
CaHM000	—	—	—	42.8	38.0	8.3	43.4	53.0	16.9
CaHM211	—	—	—	8.3	4.7	—	6.9	3.0	—
CaHM213	—	—	—	3.5	—	—	4.8	—	—
Hβ000	663	0.58	0.20	69.0	30.9	14.3	50.6	30.1	28.9
Hβ301	523	0.59	0.16	9.5	3.5	—	14.4	9.6	7.2
Hβ311	542	0.59	0.17	8.3	1.1	—	21.1	14.4	12.1
HCLβ	561	0.48	0.17	22.6	14.3	5.9	14.4	14.4	12.6
Hβ-HFS	530	0.51	0.16	88	59	35	28	28	23
HFSβ	415	0.45	0.13	52.3	23.8	11.9	13.2	13.2	15.7
USY311	744	0.09	0.33	135.5	80.8	71.3	9.6	6.0	3.6
ZSM-5	372	0.11	0.15	64.2	42.8	26.1	14.4	10.8	7.2
MCM-22	503	0.61	0.16	64.2	40.4	26.1	21.1	19.3	19.3

[a] Calculated by using absorption coefficients determined elsewhere (31).

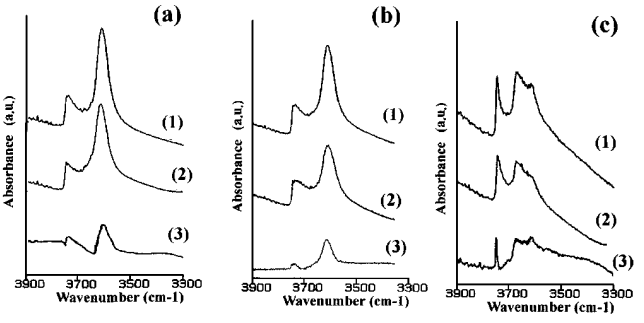

FIG. 2. IR spectra in the OH region of the mordenite samples: (1) before adsorption of pyridine, (2) after adsorption of pyridine at 523 K, and (3) the difference (1)-(2). (a) HM000, (b) HM010, and (c) HM201.

sites in these samples was not easily accessible to the pyridine molecules. This fact can be explained, assuming that a fraction of the acidic hydroxyls are located in the sidepockets of the mordenite structure and they may present accessibility problems for pyridine adsorption. In the case of HM201, partial blockage of the pores by highly condensed EFAL species generated in the steam treatment will also contribute to reduce the accessibility of the Brönsted sites to pyridine. The IR spectrum of this sample (Fig. 2c) shows, besides the band at ca 3610 cm^{-1} associated to bridging OH groups, a new broad band at ca 3670 cm^{-1} assigned to hydroxyls associated with EFAL (21). This band almost disappeared after acid leaching of HM201 (sample HM211), confirming that most of these species were removed during the treatment. Moreover, in the case of samples HM211 and HM213, almost all the bridging hydroxyls vibrating at ca 3610 cm^{-1} interacted with pyridine, since both the leaching of the condensed-type EFAL generated by steaming and the increase of the mesoporosity (Table 2) allowed the probe molecule to reach the previously inaccessible sites.

As seen in Table 2, the number of Brönsted acid sites is, as expected, lower in the dealuminated samples than in the parent HM000 and decreases as the degree of dealumination increases (HM010 > HM211 > HM213). Furthermore, it is observed that the Brönsted acidity increased after acid leaching of the steamed HM201 sample, which is probably due to the removal of condensed-type EFAL species that were blocking the zeolite pores, together with the removal of cationic EFAL species which were neutralizing part of the acid sites in HM201. The acid-washed HM010 sample presents a concentration of Brönsted acid sites retaining pyridine at 523 K similar to that of the sample HM000, but the latter contains a higher amount of strong Brönsted sites retaining pyridine at even higher temperatures. Finally, when compared to the corresponding protonic samples, it can be seen that some of the Ca-exchanged samples show a larger amount of Brönsted acid sites but, in general, a lower concentration of sites retaining pyridine at higher temperatures, suggesting a lower acid strength of the Ca-mordenite samples.

In the case of the zeolite beta samples, practically all the acid sites were accessible to the pyridine molecules during the IR experiments. The tridimensional pore system of this zeolite, in addition to the very small size of the crystallites, may have contributed to make their sites more accessible to the base as compared to mordenite.

As expected, dealumination of the sample Hβ000 lowered the concentration of Brönsted sites whatever the treatment used. However, significant differences in the zeolite properties arise when comparing samples dealuminated by different procedures. Thus, dealumination by steaming (sample Hβ301) results in a much lower density of acid sites as compared to the samples dealuminated by acid (sample HCLβ) or ammonium hexafluorosilicate (sample HFSβ) treatments. Since the steamed sample contains all the EFAL generated during the dealumination treatment, its lower acidity may be ascribed to blocking of acid sites by highly polymerized EFAL species, and probably also to the neutralization of part of the framework charge by cationic-type EFAL species, as was observed for the mordenite samples. Although acid leaching of the steamed Hβ301 sample removed part of the EFAL, as previously discussed, the Brönsted acidity hardly changed and, instead, an increase of the Lewis acid sites concentration occurred. Usually, Lewis acid sites in zeolites are associated to EFAL species, and therefore a decrease in the number of such sites could be expected when the EFAL is removed, which is not the case with sample Hβ311. The increase of Lewis acidity may be explained by considering a redispersion of the EFAL remaining in the zeolite after the acid treatment. The fact that no increase in Brönsted acidity is observed for Hβ311 as compared to Hβ301 may indicate that cationic-type EFAL species, that were neutralizing part of the sites in the latter sample, were not effectively removed during the acid treatment.

Moreover, it is seen in Table 2 that sample HFSβ presents a higher concentration of Brönsted acid sites than sample HCLβ, despite the fact that these two zeolites should contain low amounts of EFAL, according to the SAR values given in Table 1. As suggested above, this could be ascribed to the difficulty of removing cationic EFAL species by the acid treatment, whereas this type of species are more efficiently removed during the HFS treatment.

Finally, as with the other zeolitic structures, results in Table 2 show that USY311 has a high BET specific area and the highest concentration of Brönsted acid sites (Table 2) at the three desorption temperatures studied, which can be explained by its higher density of framework Al (lower SAR) (Table 1). The MCM-22 sample has a mesopore volume and a Brönsted acid strength distribution very close to that of the medium pore ZSM-5, but the former has a higher BET surface area and micropore volume. The Brönsted acidity of MCM-22 is comparable to that of the parent Hβ000 sample, although the former retains a higher amount of pyridine at

TABLE 3

Catalytic Results Obtained for the Cracking of *n*-Heptane on the Different Mordenite and Beta Samples

Sample	Activity at t = 3 min (μmol/g · min)	Deactivation coefficient (Voorhies)
HM000	1035	1.08
HM010	835	1.03
HM201	36.1	0.44
HM211	333	0.43
HM213	2.97	0.12
Hβ000	816.0	0.51
Hβ301	42.1	0.34
Hβ311	38.0	0.30
HCLβ	114.4	0.25
Hβ-HFS	382.2	0.45
HFSβ	144.3	0.20

the highest desorption temperatures (623–673 K), suggesting that it has a larger fraction of Brönsted sites with a high acid strength.

3.2. Cracking of n-Heptane

The acidic properties of the samples were also evaluated using the cracking of *n*-heptane at 623 K as a model reaction. It is well known that cracking of normal paraffins requires strong acid sites, and therefore this reaction can be used to complement the acidity results obtained by IR-pyridine.

The cracking results obtained for the mordenite and beta catalysts are summarized in Table 3, where the initial activity and the deactivation coefficient were both obtained by fitting the activity versus reaction time data to the Voorhies equation.

It can be recognized from Table 3 that sample HM000 is the most active one in the mordenite series. The steamed HM201 sample is much less active than HM211, which can be attributed to the negative influence of highly condensed EFAL species, as discussed before. Furthermore, the strongly dealuminated HM213 sample gives, as expected from its very low acidity, the lowest cracking activity. Similar results have been discussed in greater detail by Fernandes *et al.* (24).

With respect to the zeolite beta series, one may realize from Table 3 that dealumination of sample Hβ000, either by hydrothermal or chemical treatments, produces samples with a decreased catalytic activity and that steaming leads to the least active samples among those with similar framework SAR. Moreover, elimination of cationic EFAL in Hβ000 by HFS treatment (sample Hβ-HFS) reduces the catalytic activity, even though the total amount of Brönsted sites was seen to increase.

In Fig. 3 the initial cracking activity of the mordenite and beta samples is plotted versus the concentration of strong Brønsted acid sites, taken as those retaining pyridine at 623 K, which are expected to be the active sites for the cracking reaction. As can be observed, a good correlation is obtained for the mordenite series. Such correlation is also observed for the beta samples, except for the sample Hβ000, which shows a much greater activity than expected. These results indicate that some of the Brönsted acid sites in this sample have a higher turnover number for the cracking reaction. This fact, together with the characterization results discussed above, strongly suggests that some cationic EFAL species having strong Lewis acidity present in Hβ000 must be interacting with the structural Brønsted acid sites, enhancing their acid strength through a synergetic effect (25, 26) and, consequently, making them much more active for *n*-heptane cracking. This phenomenon has been already observed for the same series of samples during the hydroisomerization of C_5/C_6 *n*-paraffins (27) and the alkylation of isobutane with 2-butene (28), both reactions taking place, as the *n*-heptane cracking, on strong Brönsted acid sites. It can also be seen from Fig. 3 that the Brönsted sites of mordenite are intrinsically more active for heptane cracking than those of beta.

It can also be seen in Table 3 that the dealuminated samples were more stable than the starting materials, the effect being more evident for the mordenite series. In the case of the zeolite β samples, the increase of stability with dealumination can be explained by a reduction of the density of acid sites which may reduce the extent of bimolecular processes like those leading to coke formation and, hence, to catalyst deactivation. For mordenites, two factors are probably determining the deactivation rate of the samples. One of them may be the reduction of acid site density, as explained above, and the other could be the formation of mesopores that will connect the monodimensional 12MR channels of the mordenite and will reduce its sensibility to

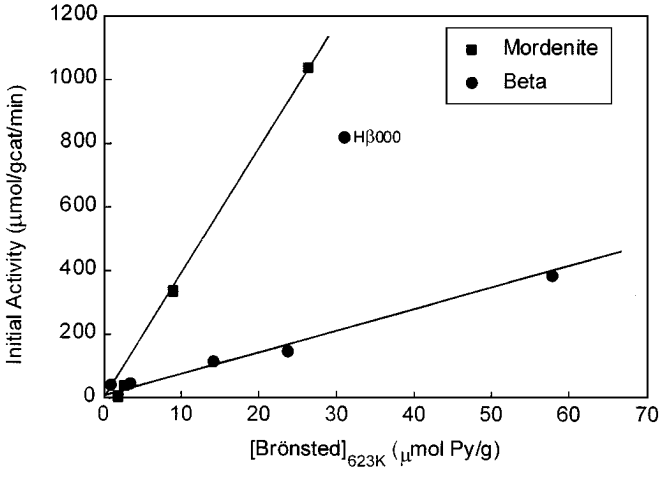

FIG. 3. Initial *n*-heptane cracking activity as a function of the concentration of strong Brönsted acid sites determined after desorption of pyridine at 623 K.

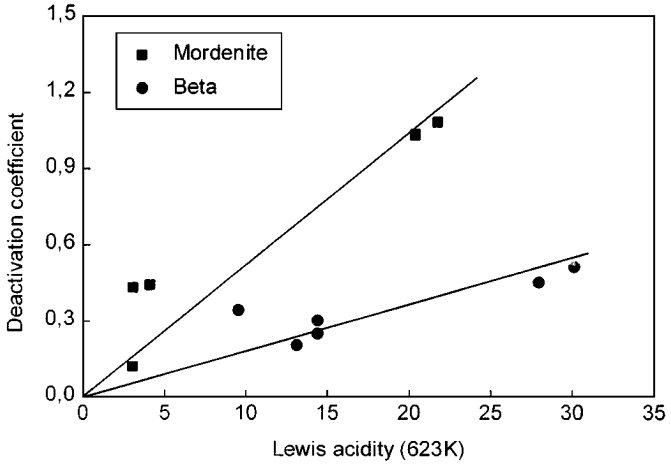

FIG. 4. Deactivation coefficients for *n*-heptane cracking on mordenite and beta samples as a function of the concentration of strong Lewis acid sites as determined by IR-pyridine.

pore blocking by coke deposits. Furthermore, a good linear relationship is observed for the two series of zeolites when the deactivation coefficient is plotted against the amount of strong Lewis acid sites as determined by IR after desorbing pyridine at 623 K (Fig. 4). This suggests that strong Lewis acid sites may increase the deactivation rate of the zeolites by enhancing coke formation through dehydrogenation and cyclization reactions, as has been suggested by some authors (29, 30).

3.3. Hydroisomerization of Ethylbenzene on Pt/zeolite Catalysts

3.3.1. Preliminary experiments. Initially, a sample of HM211 was directly impregnated with hexachloroplatinic acid and compared to a physical mixture of HM211 and Pt/Al_2O_3, prepared as described in Section 2.1, both catalysts having 0.30 wt% Pt. The former showed very low activity for ethylbenzene hydroisomerization at 653 K and very low xylene yields, dealkylation and disproportionation being the main reactions observed. Meanwhile the composite Pt/Al_2O_3 + zeolite catalyst exhibited xylene yields which were an order of magnitude larger.

The determination of the metallic area by hydrogen chemisorption revealed that platinum was better dispersed over the alumina (79%) than over the zeolite sample (9.6%). Since the hydroisomerization of ethylbenzene to xylenes is a bifunctional reaction requiring an adequate balance between acidic and metallic sites, this higher dispersion of platinum over the Al_2O_3 support may explain why the hybrid catalysts (Pt/Al_2O_3 + zeolite) present higher xylene yields.

When catalysts containing only the acid function (zeolite) were used, disproportionation and dealkylation of ethylbenzene were the main reactions observed and only traces of hydroisomerization products (selectivity to xylenes = 0.2%) were obtained, while a fast deactivation of the catalyst was also observed. On the other hand, when the reaction was performed over the Pt/Al_2O_3 component, practically only C_8 naphthenes were obtained at 653 K while at 693 K, besides naphthenes, small amounts of benzene, toluene, and cracked products were also observed.

Additional experiments were made to determine the optimum amount of platinum in the hybrid Pt/Al_2O_3 + mordenite catalysts with respect to the xylenes yield. For this purpose, the overall amount of platinum in the final catalyst was varied by using different proportions of the two components. For the catalysts with 1.0 wt% Pt, a Pt/Al_2O_3 component containing 2.0 wt% Pt was used. The results obtained at 693 K and WHSV = 10 h^{-1} are presented in Fig. 5 for the HM000, HM010, and HM211 based catalysts. These samples were selected because of their very distinct activity and selectivity during ethylbenzene (EB) conversion. This figure shows that a maximum yield of xylenes was observed at a Pt content of about 0.45 wt% (Fig. 5b) and that the EB conversion showed a similar behavior (Fig. 5a) or hardly changed at higher Pt loadings. Moreover, the yield of disproportionation (benzene + diethylbenzene) and dealkylation (benzene + light compounds) products decreased when the Pt content increased.

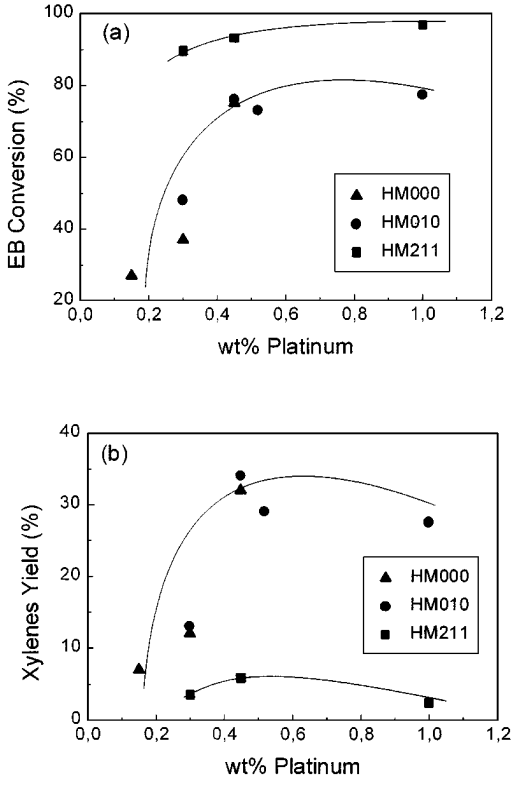

FIG. 5. Conversion of ethylbenzene (a) and yield to xylenes (b) for HM000-, HM010-, and HM211-based catalysts as a function of Pt content at WHSV = 10 h^{-1} and 693 K.

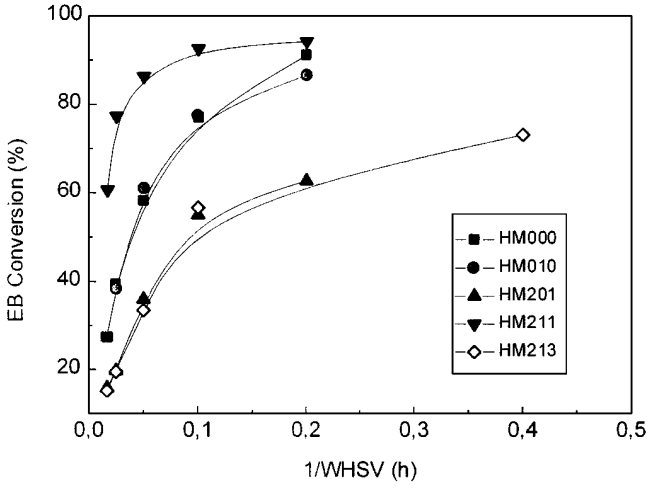

FIG. 6. Total conversion of ethylbenzene against space time (1/WHSV) for the Pt/Al_2O_3-mordenite catalysts (0.45 wt% Pt) at 693 K.

3.3.2. Mordenite-based catalysts. Based on the results presented in the previous section, the following catalytic studies were performed using hybrid Pt/Al_2O_3 (1 wt% Pt) + zeolite catalysts containing no noble metal. Therefore, the final catalyst composed by Pt/Al_2O_3 + zeolite has a global Pt content of 0.45 wt%.

Figure 6 shows the conversion of EB as a function of 1/WHSV for the different mordenite-based catalysts at 693 K. The HM211 based catalyst was the most active, despite the fact that this zeolite presented lower Brönsted acidity (Table 2) and lower activity for *n*-heptane cracking (Table 3) than the HM000 sample. This might indicate that there are other factors, in addition to acidity, that determine the activity of these catalysts for EB conversion. One of these factors could be the access of the reactant molecules to the active sites in the zeolite. The IR data had already revealed the existence of some Brönsted acid sites that were inaccessible to pyridine at 523 K, especially in the case of HM000, HM010, and HM201 which had low mesopore volumes (Table 2). Since the ethylbenzene molecule is even larger than the pyridine molecule, it might be possible that not all the acid sites detected by pyridine adsorption were accessible to the EB molecules. If this is so, then the higher activity of HM211 with respect to HM000 might be ascribed to the increased mesoporosity produced after the steam and acid leaching treatments, while both a higher mesoporosity and a greater acidity may account for the higher EB conversion obtained for HM211 with respect to HM201. Moreover, the highly dealuminated HM213 catalyst presented an activity similar to that of the steamed HM201 sample, despite the lower acidity of the former, as determined by both pyridine adsorption and *n*-heptane cracking. The higher mesoporosity and low EFAL content of the former catalyst may have contributed to its relatively high activity for EB conversion.

The yield of the main reaction products is presented in Fig. 7 as a function of EB conversion for the mordenite based catalysts. In all cases, xylenes, C_6–C_8 naphthenes, and diethylbenzene (DEB) appear as primary products, with a certain character of instability at EB conversions above 50–60%. On the other hand, C_3–C_8 aliphatics (mainly produced by ring opening and cracking of naphthenes), benzene, and toluene are all secondary products as they start to be formed at higher EB conversions. Besides these products, small amounts of trimethylbenzenes (TMB), formed by disproportionation of xylenes, and C_{10+} aromatics were also observed in the reaction products (not shown in Fig. 7). According to the above results, a simplified reaction scheme for the transformation of EB is presented in Fig. 8.

Despite the differences in activity observed for the mordenite catalysts, the xylenes yield (Fig. 7a) increases with conversion and is very similar for all samples up to a conversion level of about 60%, with the exception of HM211 which, as shown before, gave the highest EB conversion. This catalyst displays a poor isomerization selectivity, and produces high amounts of cracking products, benzene and DEB, as compared to the other mordenite samples. This indicates that dealkylation and disproportionation of EB, together with an extensive cracking of the C_6–C_8 naphthenes formed by hydrogenation of the respective aromatics, were the major reactions occurring on this catalyst. As discussed before, sample HM211 would favor the accessibility of EB to the acid sites, owing to its high mesoporosity and low EFAL content. Thus, and from the point of view of the EB molecules, this sample would contain a higher concentration of acid sites, which could explain the higher extent of cracking of the primary naphthenes, as well as dealkylation of the alkylaromatics before they can desorb to the gas phase. Moreover, this zeolite would present lower steric restrictions for the bimolecular processes, such as EB disproportionation, to occur in the zeolite pores, thus producing higher levels of DEB (Fig. 7f). The fact that the highly dealuminated HM213 catalyst, also having a high degree of mesoporosity (Table 2) and low EFAL content, does not favor these secondary reactions as HM211 does, might be ascribed to its very low acidity (Table 2).

The effect of cation exchange on the selectivity to xylenes was studied with Ca-mordenite physically mixed with the Pt/Al_2O_3 (0.6 wt% Pt) component so as to obtain a total Pt content of 0.30%, as already described in the experimental section. For a reaction temperature of 653 K, Fig. 9 shows that for all three zeolites a significant increase in the isomerization selectivity is observed after the Ca-exchange, in the full range of EB conversions studied. This increase was particularly notorious for the most dealuminated CaHM211 and CaHM213 samples and may be ascribed to a strong reduction of the consecutive cracking reactions of the

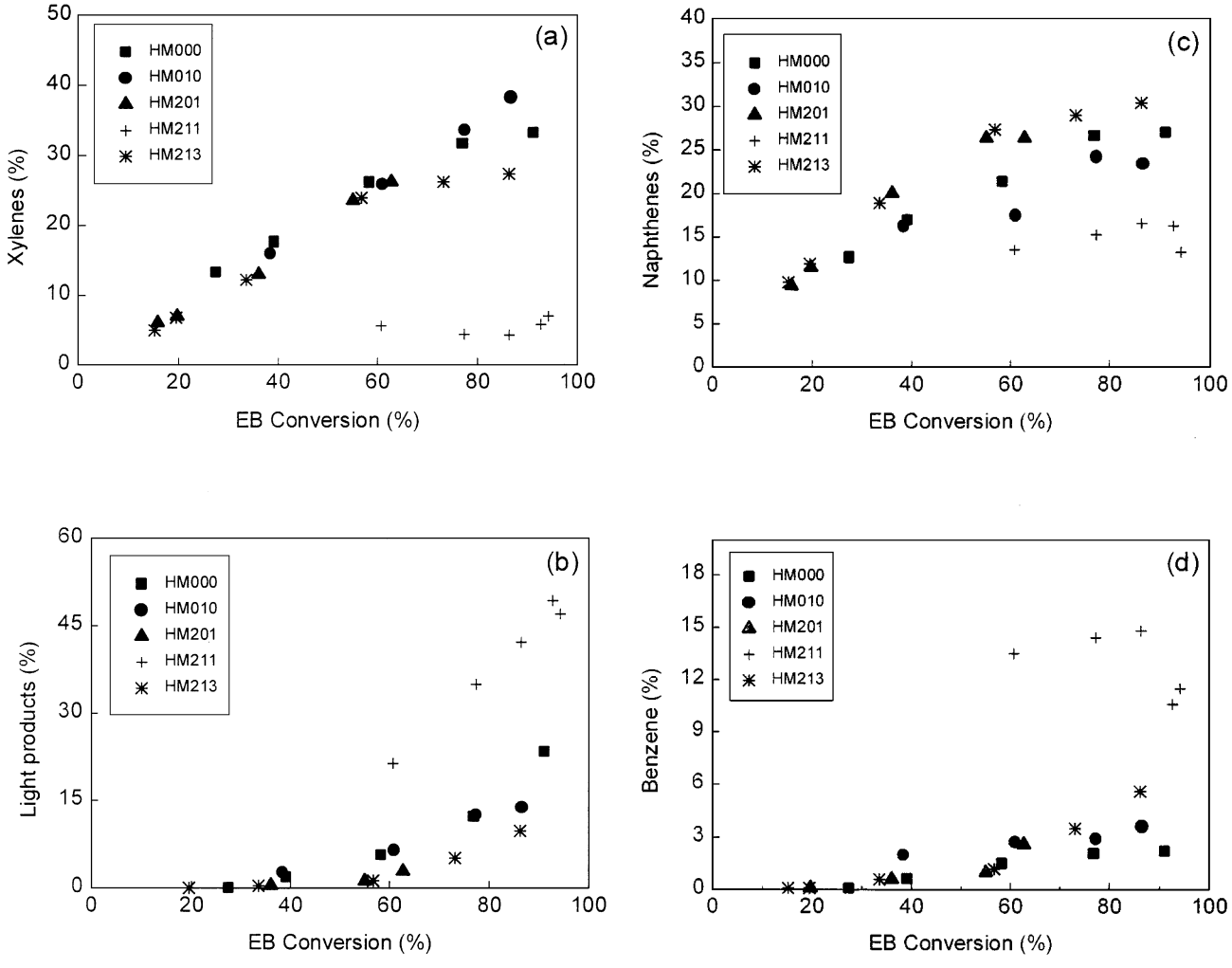

FIG. 7. Yield of the main reaction products against the EB conversion obtained at 693 K for the Pt/Al_2O_3-mordenite catalysts (0.45 wt% Pt).

naphthene intermediates while favoring the desired isomerization reaction. Although the calcium exchange step reduced the overall activity of all the samples, an increase in xylene yield was observed for the most dealuminated ones.

These catalysts were also studied at higher reaction temperatures, and the corresponding selectivities to xylenes calculated at 50% EB conversion are given in Fig. 10 as a function of temperature. As seen there, the benefit of Ca-exchange is, at higher temperatures, maintained for the most dealuminated HM211 and HM213 catalysts, but this was not the case for the HM000 sample. This catalyst was more selective to xylenes than its Ca-exchanged counterpart at temperatures of 673 K and above.

3.3.3. Beta-based catalysts. The activity of the catalysts (0.45 wt% Pt) prepared from zeolite beta, given as the EB conversion at different 1/WHSV at 693 K, is shown in Fig. 11. In this case, the steamed Hβ301 sample shows a catalytic activity comparable to that of the sample Hβ000 and higher than that of the samples dealuminated by either acid or HFS treatments. In fact, the latter sample (HFSβ) presents the lowest activity for EB conversion, despite its high acidity as measured by IR-pyridine. As was shown in Table 2, HFSβ presented the lowest surface area and micropore volume, which was attributed to pore blocking by silica deposits produced during the HFS treatment, as already discussed. In principle, one would expect lower diffusional restrictions for the ethylbenzene molecules in the tridirectional structure of zeolite beta as compared to the monodimensional channels of mordenite. However, the low ethylbenzene conversion obtained for HFSβ probably points to some diffusional restrictions caused by the silica deposits. In a former work (27), the same zeolite beta samples studied here were tested in light *n*-paraffin (LSR) hydroisomerization, and it was observed that the HFSβ sample was more active than Hβ301 and Hβ311 samples. As can be seen in Table 3, HFSβ also appeared to be

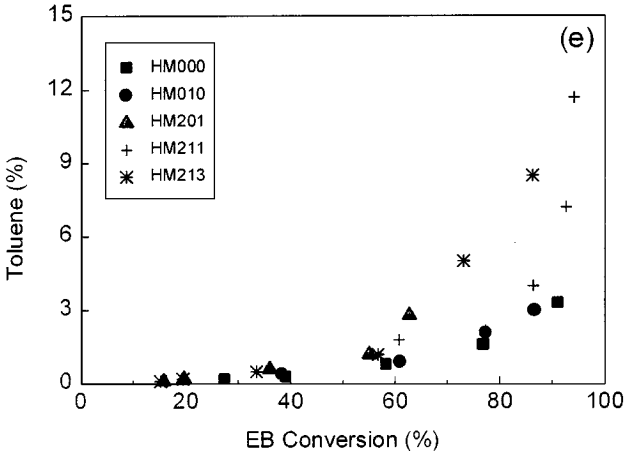

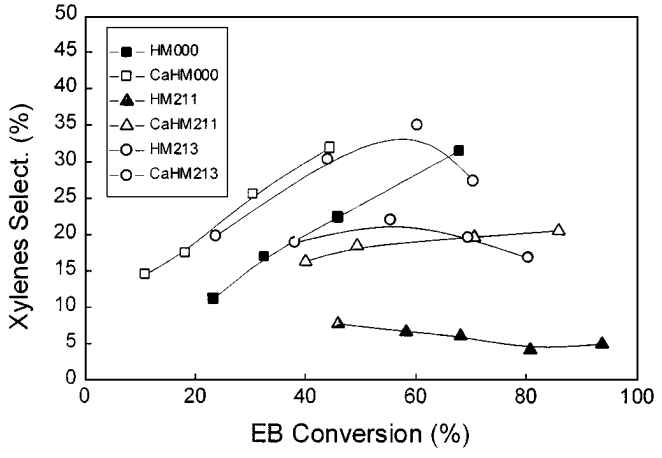

FIG. 9. Xylenes selectivity during EB hydroisomerization over Pt/Al_2O_3-calcium exchanged mordenites (0.30 wt% Pt) at 653 K.

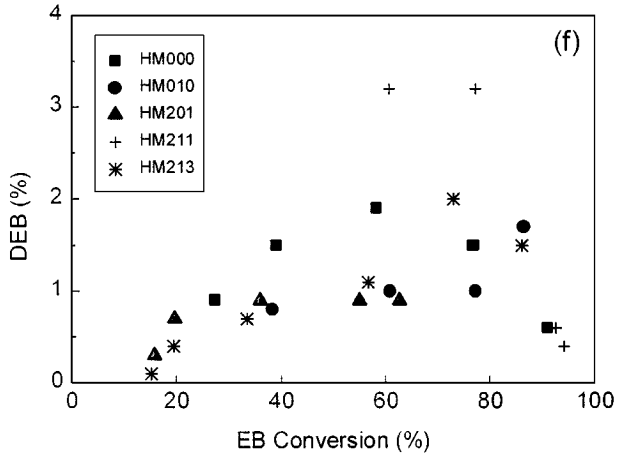

FIG. 7—*Continued*

more active in *n*-heptane cracking than Hβ301 and Hβ311. These results suggest that the acidity of the zeolite mainly determines the catalytic activity in both LSR hydroisomerization and *n*-heptane cracking reactions, whereas the access of the reactant molecules to the active sites also seems to play a significant role during the conversion of EB on Pt/Al_2O_3-zeolite β catalysts.

The yield to the main reaction products as a function of EB conversion is given in Fig. 12 for the Pt/Al_2O_3-zeolite β catalysts. It has to be noted that the beta catalysts produced, in general, higher yields of DEB than the mordenite samples. This can be ascribed to the more open structure of zeolite beta and its larger void spaces in which the bimolecular transition state needed for the disproportionation reaction can be better accommodated.

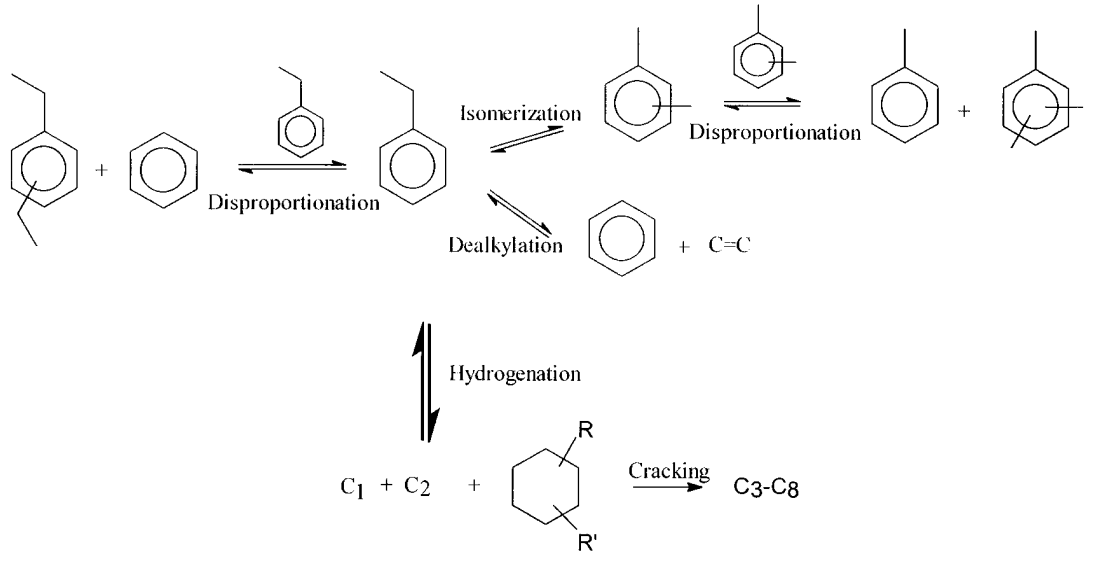

FIG. 8. Proposed reaction scheme for the hydroisomerization of ethylbenzene on bifunctional Pt/zeolite catalysts.

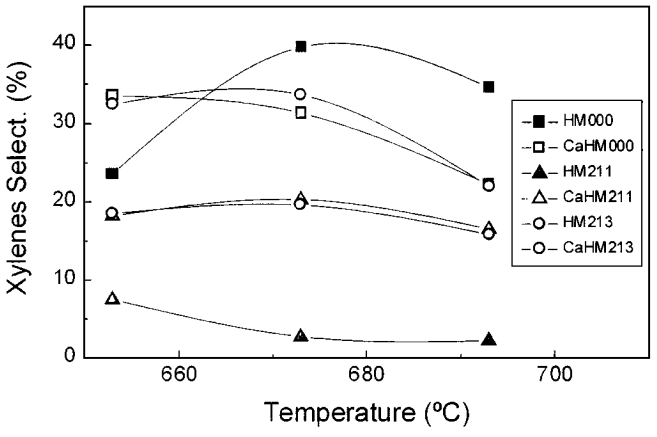

FIG. 10. Influence of temperature on xylene selectivity during EB hydroisomerization over Pt/Al_2O_3-calcium exchanged mordenites (0.30 wt% Pt) obtained at 50% EB conversion.

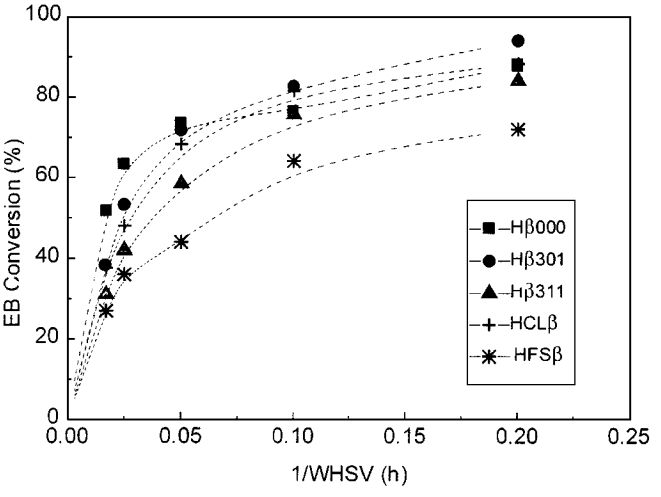

FIG. 11. Total conversion of ethylbenzene against space time (1/WHSV) for the Pt/Al_2O_3-zeolite β catalysts (0.45 wt% Pt) at 693 K.

It can also be observed in Fig. 12 that samples Hβ311 and Hβ301, prepared by hydrothermal treatment of Hβ000 and having low Brönsted acidity and high mesopore volumes, give the highest yield of xylenes (Fig. 12a) within the beta series. Only for those two samples the xylene yield clearly increases with EB conversion. On the other hand, sample Hβ000 produces large amounts of light products and benzene (Figs. 11b–d). As discussed before, this zeolite contains Brönsted acid sites whose acid strength was greatly enhanced by the interaction with cationic EFAL species. Contrary to the steamed samples, those dealuminated by acid (HClβ) and hexafluorosilicate (HFSβ) treatments give high yields of benzene and DEB (Figs. 12d, f) and low yields of xylenes.

These results suggest that the formation of xylenes in Pt/Al_2O_3-zeolite β catalysts is favored by a low acidity and a high degree of mesoporosity, factors which are characteristic of the zeolites dealuminated by steaming, i.e. Hβ301 and Hβ311. On the other hand, the presence of very strong acid sites, as in the Hβ000 sample, causes a very high activity for dealkylation and for cracking of the naphthene intermediates, and consequently a low isomerization activity. Moreover, the EFAL-free dealuminated samples, still having a large concentration of Brönsted acid sites, promote EB dealkylation and disproportionation, rather than isomerization.

3.3.4. Influence of zeolite structure. Finally, the influence of zeolite structure on the catalytic performance of bifunctional Pt/Al_2O_3-zeolite composites (0.45 wt% Pt) for the hydroconversion of EB at 693 K is presented in Table 4. It is seen there that large pore (beta, mordenite, and USY) are more selective to xylenes than medium pore zeolites, at least under the reaction conditions used here. Among the large pore zeolites studied, mordenite and beta show a better catalytic performance, with a selectivity to xylenes of ca 40% at a conversion level of 60%. The USY zeolite used gives less xylenes and many more gases (ca 26% selectivity at 60% conversion) than the above two zeolites, which can be ascribed to its much greater number of acid sites, as observed by IR-pyridine (Table 2).

On the other hand, the medium pore ZSM-5 catalyst shows the highest EB conversion at constant WHSV, but its selectivity to xylenes is very poor. At 60% conversion

TABLE 4

Ethylbenzene Conversion (at WHSV = 10 h^{-1} and 693 K) and Product Selectivities Obtained at ca 60% Conversion for the Pt/Al_2O_3-zeolite Catalysts (0.45 wt% Pt)

Sample	Conversion	Selectivity (%molar)					
		Xylene	Gas	Naphthenes	Benzene	Toluene	DEB
HM000	76.3	43.9	11.0	36.2	2.7	1.7	2.7
ZSM-5	97.3	9.1	14.1	14.7	60.7	5.9	2.6
Hβ311	75.7	38.0	9.9	29.2	6.7	3.5	7.1
MCM-22	52.5	16.8	4.1	9.2	36.8	6.9	15.5
USY311	59.8	27.5	26.1	25.4	8.0	5.7	3.9

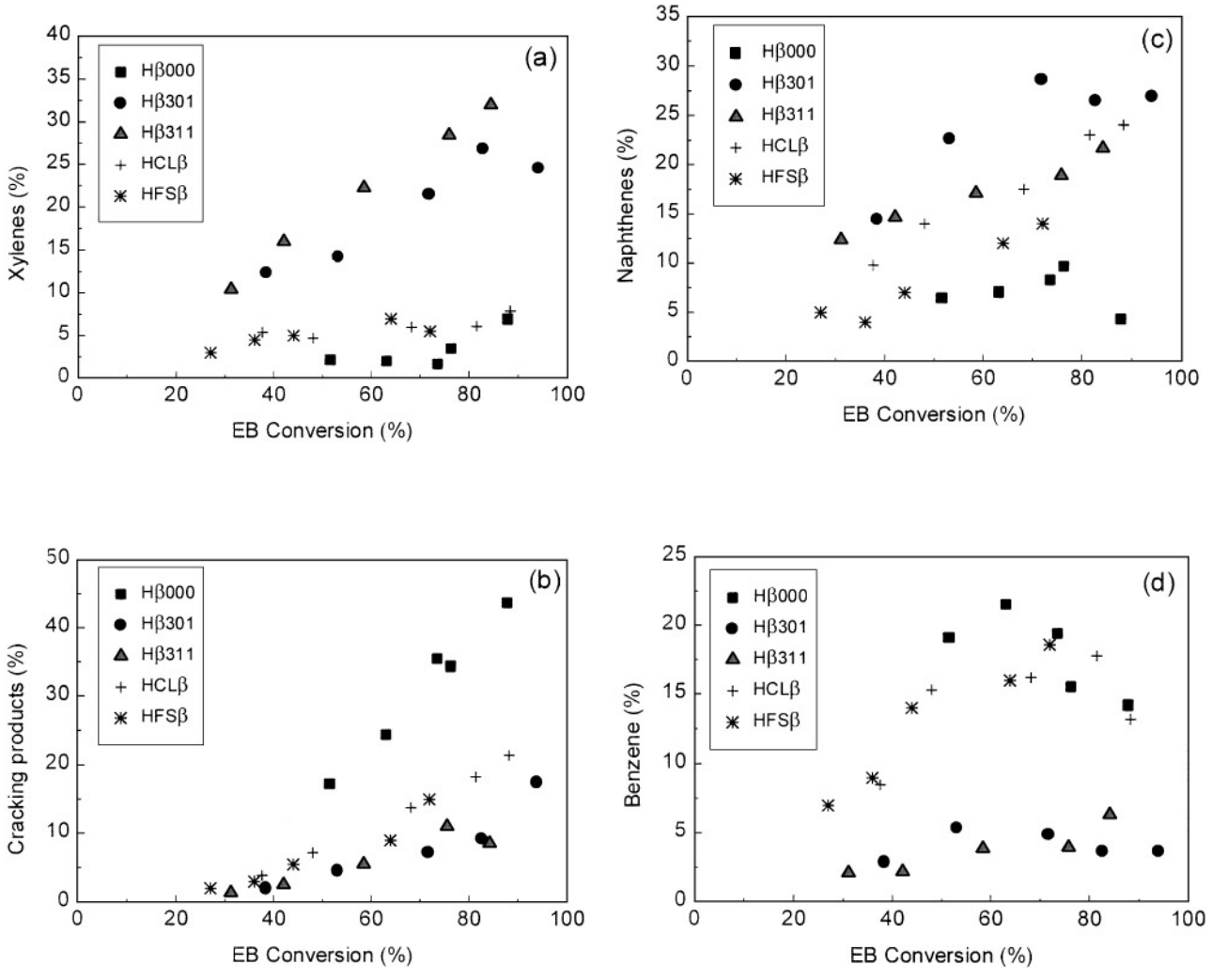

FIG. 12. Yield of the different reaction products as a function of EB conversion at 693 K for the Pt/Al_2O_3-beta catalysts (0.45 wt% Pt).

this zeolite gives about 60% selectivity to benzene, indicating a very high dealkylation activity. This can be ascribed to both the high concentration of strong Brönsted acid sites (Table 2) and to the presence of narrower pores which increases the steric restrictions for the formation of the naphthene intermediates. The MCM-22 zeolite, presenting a peculiar pore architecture formed by two independent 10 MR systems of channels, one of them sinusoidal and the other containing large cavities delimited by 12 MR windows, also shows low xylene yields and high selectivities to benzene and diethylbenzene, suggesting that the large intermediates formed during disproportionation could be easily accommodated in its large supercages. It can be concluded that the EB hydroisomerization reaction requires large pore zeolites, which can accommodate in the inner pores the naphthene intermediates that will lead to the desired xylenes after expansion and contraction of the ring (2–5) and can also allow a fast diffusion of the products to the gas stream.

4. CONCLUSIONS

A series of mordenite and beta zeolites having different chemical compositions (framework and extraframework Al content) and physicochemical properties have been prepared by postsynthesis methods, i.e., steaming, acid leaching (HCl), and ammonium hexafluorosilicate (HFS) treatments. Then, bifunctional catalysts have been generated by mixing the zeolite with a Pt/Al_2O_3 component and their activity measured for the hydroconversion of EB at 15 bar total pressure and reaction temperatures in the range of 653–693 K.

All the Pt/Al_2O_3-mordenite catalysts presented significant activity for EB conversion and high selectivity to xylenes (about 40% at 60% conversion) under the above reaction conditions, with the exception of the catalyst prepared from the mordenite that was steamed and acid washed with a HCl aqueous solution (HM211). Due to its

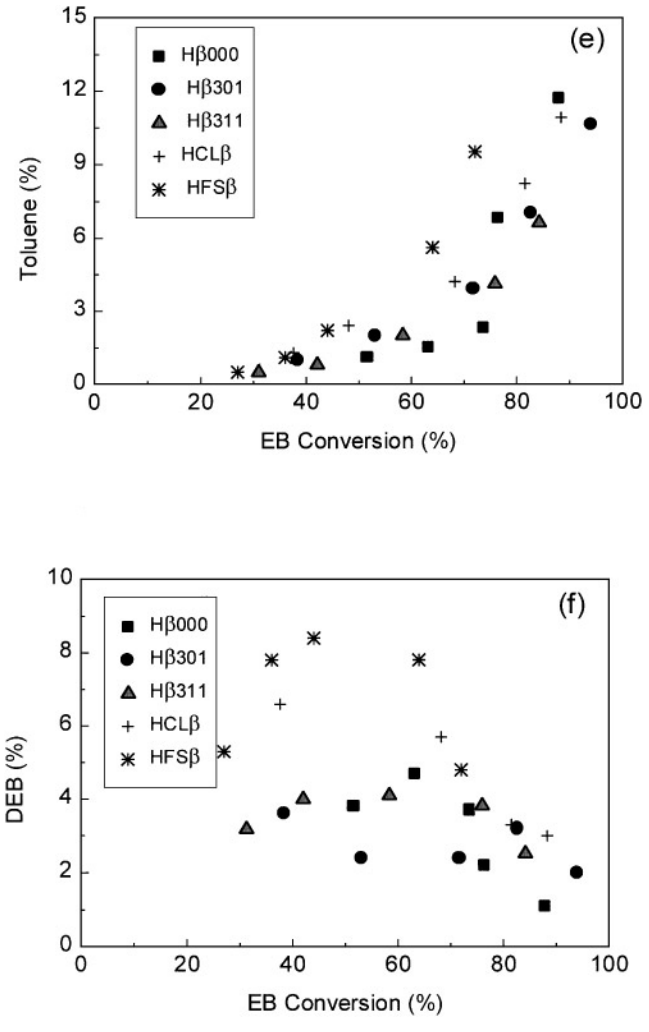

FIG. 12—*Continued*

relatively high mesoporosity (as compared to the other mordenite samples) and low EFAL content, this sample probably provides EB a better access to acid sites, and therefore, from the point of view of the reactant, this catalyst would be more acidic. This probably brings about a higher extension of the secondary reactions leading to a low yield of xylenes. The high selectivity observed for the HM000 sample, having a high density of Brönsted acid sites as measured by IR-pyridine, may be ascribed to its low mesoporosity, which certainly determines that not all the acid sites detected by pyridine are accessible to the EB molecules, and thus it behaves as a zeolite with a reduced density of acid sites. Moreover, when part of the protons in the mordenite samples were exchanged by Ca^{2+} cations, thus reducing their acid strength, the selectivity to xylenes significantly increased at 653 K. The benefit of reducing acid strength through Ca^{2+} exchange on the selectivity is, at higher temperatures, maintained for the most dealuminated HM211 and HM213 catalysts.

In the case of the Pt/Al_2O_3-zeolite β catalysts, higher xylene yields were obtained with the zeolites prepared by steaming (Hβ301) and steam + acid leaching (Hβ311) of the parent sample. These catalysts contain a higher degree of mesoporosity and a reduced density of Brönsted acid sites, as compared to the other beta samples, which may favor the formation of the voluminous naphthene intermediates and prevent the EB dealkylation and cracking reactions.

Finally, it was seen that the pore structure greatly influences the product selectivity, with large pore zeolites being more selective to the desired isomerization products (xylenes) than zeolites with narrower pores. The order of selectivity found was: mordenite (HM010) > beta (Hβ311) > USY > MCM-22 > ZSM-5.

From the above results it could be concluded that the hydroisomerization of EB to xylenes on bifunctional Pt-zeolite catalysts is favored in zeolites with large pores and a high degree of mesoporosity, and presenting a reduced density of Brönsted acid sites accessible to the EB molecules. These two factors will allow a fast diffusion of the products out of the zeolite structure, decreasing the probability for secondary reactions to occur.

ACKNOWLEDGMENTS

Financial support by Conselho Nacional de Desenvolvimento Científico e Tecnológico (CNPq/Brazil) and by Comisión Interministerial de Ciencia y Tecnología (CICYT) of Spain (Project MAT 94-0166) is gratefully acknowledged.

REFERENCES

1. Hsu, Y. S., Lee, T. Y., and Hu, H. C., *Ind. Eng. Chem. Res.* **27**(6), 942 (1988). [Corma, A., *Chem. Rev.* **95**, 559 (1995)]
2. Röbschläger, K. H., and Christoffel, E. G., *Ind. Eng. Chem. Prod. Res. Dev.* **18**, 347 (1979).
3. Gnep, N. S., and Guisnet, M., *Bull. Soc. Chim. Fr.* **5-6**, 429 (1977).
4. Gnep, N. S., and Guisnet, M., *Bull. Soc. Chim. Fr.* **5-6**, 435 (1977).
5. Röbschläger, K. H., and Christoffel, E. G., *Can. J. Chem. Eng.* **58**, 517 (1980).
6. Ribeiro, M. F. G., D.Sc. dissertation, Universidade Técnica de Lisboa, 1989.
7. Ribeiro, M. F. G., Travers, Ch., Raatz, F., Marcilly, Ch., and Ribeiro, F. R., *in* "Zeolites: Facts, Figures, Future" (P. A. Jacobs and van Santen, Eds.), p. 1349. Elsevier Science, Amsterdam, 1989.
8. Travers, Ch., Raatz, F., Marcilly, Ch., Ribeiro, F. R., and Ribeiro, M. F. G., Europ. Patent 0363253 (1989).
9. Basset, J. M., Choplin, A., Raatz, F., Theolier, A., and Travers, C., WO 90/09845 (1990).
10. Ribeiro, M. F., Lemos, F., Ribeiro, F. R., Marcilly, Ch., Travers, Ch., and Raatz, F., *in* "Proc. Div. Petr. Chem., American Chemical Society, New York City, 1991," p. 872.
11. Benazzi, E., Tavernier, S., Beccat, P., Joly, J. F., Nedez, Ch., Besset, J. M., and Choplin, A., *in* "Prep. Div. Petr. Chem., 206th National Meeting, American Chemical Society, Chicago, 1993," p. 561.
12. Silva, J. M., Ribeiro, M. F., Ramôa Ribeiro, F., Benazzi, E., and Guisnet, M., *Appl. Catal.* **125**, 1 (1995).
13. Silva, J. M., Ribeiro, M. F., Ramôa Ribeiro, F., Benazzi, E., and Guisnet, M., *Appl. Catal.* **125**, 15 (1995).

14. Haag, W. O., and Olson, D. H., U.S. Patent 0434347 (1990).
15. Brown, L. M., and Huang, T. J., U.S. Patent 5028573 (1991).
16. Polinski, L. M., and Baird, M. J., *Ind. Eng. Chem. Prod. Res. Dev.* **24**, 540 (1985).
17. Babu, G. P., Santra, M., Shiralkar, V. P., and Ratnasamy, P., *J. Catal.* **100**, 458 (1986).
18. Bayburskii, V. L., Anokhina, T. A., Aleksandrova, I. L., and Khadzhiev, S. N., *Kinet. Katal.* **27**, 1484 (1986).
19. Ferreira, J. M. M., Ph.D. dissertation, PEQ/COPPE-UFRJ, Brazil, June 1991.
20. Corma, A., Corell, C., and Pérez-Pariente, J., *Zeolites* **15**, 2 (1995).
21. Corma, A., Fornés, V., Martínez, A., and Sanz, J., *ACS Symp. Ser.* **375**, 49 (1988).
22. Gilson, J. P., Edwards, G. C., Peters, A., Rajagopalan, K., Wormsbecher, R. F., Roberie, T. G., and Shatlock, M. P., *J. Chem. Soc., Chem. Commun.*, 91 (1987).
23. Wang, Q. L., Torrealba, M., Giannetto, G., Perot, G., Cahoreau, M., and Caisso, J., *Zeolites* **10**, 703 (1990).
24. Fernandes, L. D., Monteiro, J. L. F, Bartl, P. E., Gusmão, J., Menezes, S. C., and Cardoso, M. J. B., *Zeolites* **14**, 533 (1994).
25. Mirodatos, C., and Barthomeuf, D., *J. Chem. Soc., Chem. Commun.* 39 (1981).
26. Hong, Y., Gruver, V., and Fripiat, J. J., *J. Catal.* **150**, 421 (1994).
27. Corma, A., Martínez, A., Fernandes, L. D., Monteiro, J. L. F., and Sousa-Aguiar, E. F., *in* "Catalysis by Microporous Materials" (H. K. Beyer, H. G. Karge, I. Kiricsi, and J. B. Nagy, Eds.), p. 456. Elsevier Science, Amsterdam, 1995.
28. Corma, A. Martínez, A., Arroyo, P. A., Monteiro, J. L. F., and Sousa-Aguiar, E. F., *Appl. Catal. A: General* **142**, 139 (1996).
29. Abbot, J., and Guerzoni, F. N., *Appl. Catal. A: General* **85**, 173 (1992).
30. Niu, F., and Hofmann, H., *Appl. Catal. A: General* **128**, 107 (1995).
31. Emeis, A. C., *J. Catal.* **141**, 347 (1993).